Local structure changes of Ga during nanocrystalline formation from melt-quenched $Fe_{73}Ga_4Nb_3Si_{11}B_9$ alloys

1995 J. Phys.: Condens. Matter 7 7087

(http://iopscience.iop.org/0953-8984/7/35/016)

J. Phys.: Condens. Matter 7 (1995) 7087–7097. Printed in the UK

Local structure changes of Ga during nanocrystalline formation from melt-quenched $Fe_{73}Ga_4Nb_3Si_{11}B_9$ alloys

Makoto Matsuura†, Masaki Sakurai‡, Sang-Hyeob Kim‡, Kenji Suzuki‡ and Toshiro Tomida§

† Miyagi National College of Technology, Natori Miyagi 981-12, Japan
‡ Institute for Materials Research, Tohoku University, Sendai 980, Japan
§ Advanced Technology Research Laboratories, Sumitomo Metal Industries Ltd, 1–8 Fusocho, Amagasaki, 660, Japan

Received 20 January 1995, in final form 19 April 1995

Abstract. XAFS measurements of the Ga K edge and the Nb K edge have been carried out for amorphous $Fe_{73}Ga_4Nb_3Si_{11}B_9$ alloy after annealing at various temperatures in order to reveal the roles of Ga and Nb in the nanocrystalline formation. XAFS results show that there is no definite Ga segregation, unlike Cu in $Fe_{73.5}Cu_1Nb_3Si_{13.5}B_9$ (FINEMET). XAFS spectra of Ga for the samples annealed above the α-iron precipitation temperature, T_{x1}, indicate that Ga atoms sit substitutionally at bcc iron sites. Curve fitting analyses of the XAFS of Ga show that coordination number after annealing drops at T_{x1} but it rises again above T_{x1}, which suggests that at the beginning of α-iron precipitation, Ga atoms are inclined to be excluded toward the boundary where B and Si are much more abundant than other atoms. Such a transient exclusion effect of Ga can be attributed to the nanocrystalline formation of these alloys. Nb in $Fe_{73}Ga_4Nb_3Si_{11}B_9$ seems to play the same role as that in FINEMET, i.e. retarding crystal growth of α-iron and suppressing Fe–B compound formation.

1. Introduction

There are many amorphous alloys whose crystallization exhibits the primary type of crystallization (Köster and Herold 1981). In primary crystallization a supersaturated solid solution is precipitated at a lower temperature (T_{x1}) and subsequently some compounds are formed from remaining amorphous matrix at a higher temperature (T_{x2}). Among this type of amorphous alloy, uniform and ultrafine grains of solid solution are sometimes formed by annealing at temperatures between T_{x1} and T_{x2} for an appropriate time.

In order to reduce the grain size of the precipitated solid solution, nucleation should occur in a short time with a high frequency at a low temperature. Since the velocity of nucleation growth is slow at a low temperature, a lower nucleation temperature is preferable to increase the number of nucleation cites. Furthermore it is useful to raise T_{x2} because a temperature region of annealing, $\Delta T_x = T_{x2} - T_{x1}$, extends without being impeded by compound formation. Addition of a small amount of elements is sometimes useful for these purposes, i.e. to lower T_{x1} and raise T_{x2}. For example, the combined addition of Cu(1 at.%) and Nb(3 at.%) into $Fe_{77.5}Si_{13.5}B_9$ alloy results in the decrease in grain size of the precipitated α-iron to 10–20 nm by annealing melt-quenched amorphous ribbon at the optimum condition (Yoshizawa *et al* 1988, Yoshizawa and Yamauchi 1990). In this case Cu is believed to lower the precipitation temperature of α-iron ($=T_{x1}$) in the early stage

0953-8984/95/357087+11$19.50

of crystallization, while Nb suppresses Fe–B compound formation and consequently raises T_{x2}. Therefore 'combined' addition of Cu and Nb is necessary to obtain nanoscale grains in this alloy. In fact our previous work has directly shown evidence by x-ray absorption fine structure (XAFS) measurements that Cu atoms form fcc clusters in the amorphous matrix prior to bcc iron precipitation and local structure of Nb changes when Fe–B compounds are formed first (Kim *et al* 1993). Because Cu is insoluble in Fe, supersaturated Cu is likely to precipitate by annealing below the onset temperature of α-iron precipitation, which may promote α-iron precipitation although details on the connection between the formation of fcc-Cu clusters and α-iron precipitation have not yet been clarified. The addition of Au which is also insoluble in Fe instead of Cu has been reported to exhibit the same effects as Cu (Kataoka *et al* 1989).

Recently the same effects as for Cu in $Fe_{73.5}Cu_1Nb_3Si_{13.5}B_9$ have been found for Ga in $Fe_{73}Ga_4Nb_3Si_{11}B_9$ (hereafter FeGaNbSiB) by one of the present authors (Tomida 1994) in spite of the fact that Ga is soluble in Fe. He showed that addition of Ga (2–6 at.%) into $Fe_{77-x}Nb_3Si_{11}B_9$ lowers the precipitation temperature of α-iron and raises that of Fe–B compound formation and thereby uniform nanoscale α-iron crystallites can be obtained by appropriate annealing. Therefore the combined addition of Ga and Nb to the $Fe_{78}Si_{13}B_9$ alloy results in the improvement of its soft magnetic properties. Our main interest is why Ga addition causes lowering of the precipitation temperature of α-iron and in consequence nanocrystallites can be formed as for Cu in $Fe_{73.5}Cu_1Nb_3Si_{13.5}B_9$ even though Ga is soluble in Fe. Because of the limited amount of Ga and Nb content usual analyses are not useful to reveal the role of Ga and Nb. For this purpose we use the XAFS technique because XAFS extracts structural information around a specific atom.

2. Experiments

Ribbon samples of FeGaNbSiB were prepared by a single roll melt quenching technique. The surface velocity of the roll was about 30 m s^{-1}. The width and thickness of the ribbon samples were about 5 mm and 25 μm respectively. Chemical analysis of the ribbon samples showed their composition as Fe (72.3), Ga (4.3), Nb (2.9), Si (11.4) and B (9.1) in at.%. As a reference material for the XAFS measurements a crystalline $Fe_{99}Ga$ bulk sample was prepared by arc melting followed by 48 hour annealing at 1173 K and then water quenching. X-ray diffraction measurements for the samples used for the XAFS measurements were done using Cu Kα radiation. For XAFS and transmission electron microscope (TEM) measurements the following samples were prepared: as quenched and annealed at temperatures of 623 K, 693 K, 713 K, 723 K, 783 K and 893 K for 1 hour in an argon gas atmosphere. Foils for TEM observation were prepared by Ar ion thinning and the observation was done with an acceleration voltage of 400 kV. The XAFS measurements of the Ga and the Nb K edges of FeGaNbSiB were made by a transmission method. The fluorescence method was adopted for the Ga K edge of $Fe_{99}Ga$. All the XAFS measurements were done using synchrotron radiation in KEK PF at BL-7C. The x-ray energy was defined by an Si (111) monochromator.

3. Results

Figure 1 shows x-ray diffraction patterns for the samples of FeGaNbSiB used for the XAFS measurements. The amorphous structure of the as-quenched sample can be realized from a halo pattern. Diffraction peaks due to α-iron precipitation evolve at 723 K; at 713 K no

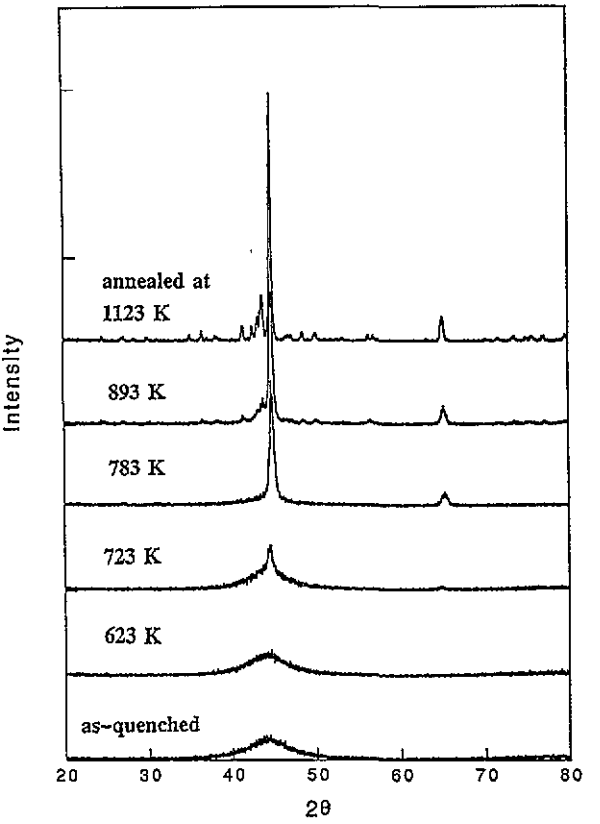

Figure 1. X-ray diffraction patterns using Cu Kα radiation for $Fe_{73}Ga_4Nb_3Si_{11}B_9$: as quenched, annealed at 623 K, 723 K, 783 K, 893 K and 1123 K.

visible changes of the halo pattern were observed, though it is not shown in this figure. The extra peaks other than α -iron observed for the samples annealed above 893 K can be identified as Fe_2B, DO_3-type FeSi and X phase which has been found recently by one of the present authors (Tomida 1994) to be a hexagonal structure with relatively large lattice parameters i.e. $a = 1.23$ nm and $c = 0.77$ nm. The lattice parameter of the precipitated α-iron is about 0.286 nm. The concentration dependence of the lattice parameter of the precipitated α-iron for $Fe_{73+x}Ga_4Nb_3Si_{11-x}B_9$ shows a decrease with increasing Si content as for Fe–Si alloys. This fact indicates that Si atoms are incorporated with precipitated α-iron. Furthermore the lattice parameter at a lower Si concentration exceeds the value for α-iron (=0.28664 nm), e.g. 0.2881 nm at $x \approx 6$. Therefore not only Si but also Ga is expected to be dissolved in the precipitated α-iron. A typical bright-field image of TEM and an electron diffraction pattern for the sample annealed at 783 K shown in figure 2 indicate fine nanograins of α-iron with about 10 nm diameter embedded in the amorphous matrix.

Figure 3 shows the result of XAFS measurements represented in terms of $k^3\chi(k)$ against k for the Ga K edge of FeGaNbSiB: as quenched and annealed at 713 K, 723 K and 893 K. The results for those samples annealed at 623 K and 783 K, which are not shown here, are quite similar to those for the samples as quenched and annealed at 893 K respectively. Figure 4 shows results of Fourier transforms of those $k^3\chi(k)$ shown in figure 3 over the k range from 2.6 to 15.5 $Å^{-1}$. Both figures 3 and 4 indicate that at 713 K which is just below the α-iron precipitation temperature (=723 K) the local structure of Ga shows a

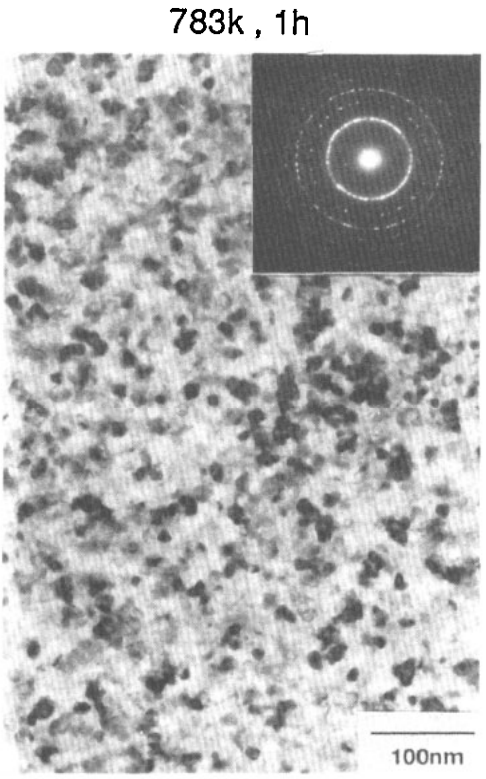

Figure 2. Bright-field image of TEM and electron diffraction pattern for the $Fe_{73}Ga_4Nb_3Si_{11}B_9$ annealed at 783 K.

rather small change compared with the as quenched one, while as soon as α-iron begins to precipitate, i.e. at 723 K, a clear change is visible. This result shows a sharp contrast to Cu in $Fe_{73.5}Cu_1Nb_3Si_{13.5}B_9$, where the local structure of Cu begins to change toward fcc structure at least 40 K below the onset of α-iron precipitation. Comparison of $k^3\chi(k)$ against k curves of the Ga K edge among $Fe_{99}Ga$ and FeGaNbSiB annealed at 893 K and the Fe K edge of pure bcc Fe, is shown in figure 5. The similarity of FeGaNbSiB annealed at 893 K to bcc $Fe_{99}Ga$ rather than bcc Fe is obvious.

Figure 6 shows the $k^3\chi(k)$ against k curves of the Nb K edge for the samples as-quenched and annealed at 783 K and 893 K of FeGaNbSiB. Even at 783 K where precipitation of α-iron has finished, the whole feature of the curve shows a quite small change from the as-quenched state but a drastic change occurs at 893 K where Fe–B compounds are formed. These XAFS results of Nb suggest that Nb is not included in the precipitated α-iron crystallites but incorporated in compounds such as Fe–B and Nb–B. Such a behaviour of Nb in FeGaNbSiB during crystallization is similar to that of Nb in $Fe_{73.5}Cu_1Nb_3Si_{13.5}B_9$.

4. Curve fitting analysis for XAFS results

There are two different ways of choosing backscattering amplitude $f(k)$ and phase shift $\phi(k)$ in curve fitting of observed EXAFS data: one is extraction from a model compound and the

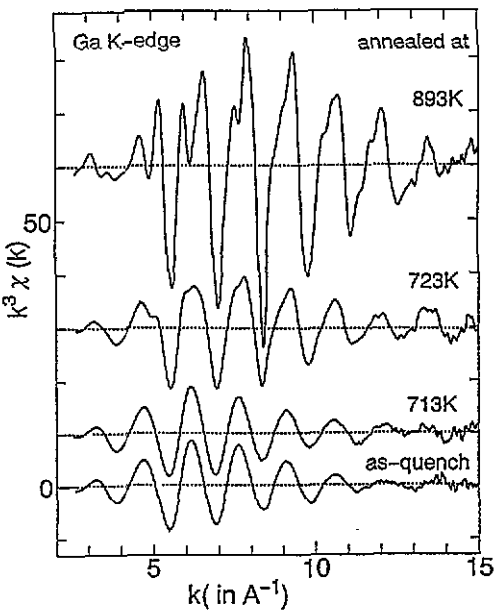

Figure 3. $k^3\chi(k)$ against k curves of the Ga K edge for $Fe_{73}Ga_4Nb_3Si_{11}B_9$: as quenched, annealed at 713 K, 723 K and 893 K.

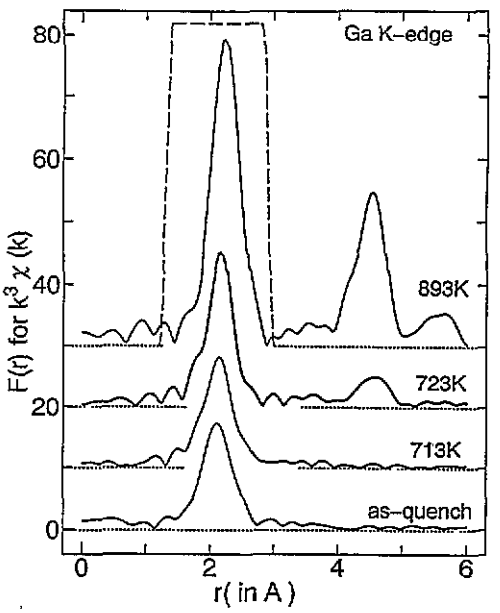

Figure 4. Fourier transforms of $k^3\chi(k)$ for $Fe_{73}Ga_4Nb_3Si_{11}B_9$: as quenched, annealed at 713 K, 723 K and 893 K. A dotted line shows a window function used for the inverse transformation.

other from a theoretical calculation. A model compound is more reliable than the theoretical calculation if a suitable model compound is available. In the present case, however, a good model compound is not available for an amorphous phase. Therefore we adopted theoretical parameters deduced by *ab initio* calculation using FEFF5 (Rehr *et al* 1991). $\chi(k)$ of the Ga K edge for two model structures were calculated: one is a single Ga atom in fcc Fe for the curve fitting of amorphous samples and another single Ga atom in bcc Fe for that of crystallized samples. $f(k)$ and $\chi(k)$ were deduced by fitting the calculated $\chi(k)$ to the following EXAFS function based on the plane wave and single-scattering approximations:

$$\chi(k) = \sum_i A_i(k) \sin \Phi_i(k) \tag{1}$$

where

$$A_i(k) = \frac{N_i}{kr_i^2} f_i(k) \exp\left[-\frac{2r_i}{\lambda} - 2\sigma^2 k^2\right] \qquad \Phi_i(k) = 2kr_i + \phi_i(k)$$

and $f_i(k)$ is the backscattering amplitude from each of N_i neighbouring ith type atoms which are placed at a distance r_i from the central atom. $\phi_i(k)$ is the composite phase shift. In the procedure of the deduction of $f_i(k)$ and $\phi_i(k)$ from the theoretical calculation using FEFF5, the k range in the Fourier transform and the r range in Fourier filtering are aligned the same as for the subsequent curve fitting of the observed data.

Anharmonicity in radial displacement needs to be considered for a disordered structure such as the present amorphous phase (see for example Eisenberger and Brown 1979). The cumulant technique can be applied to such system with anharmonic displacement (Bunker 1983). Cumulant expansion up to the fourth order was adopted as a fitting equation for the

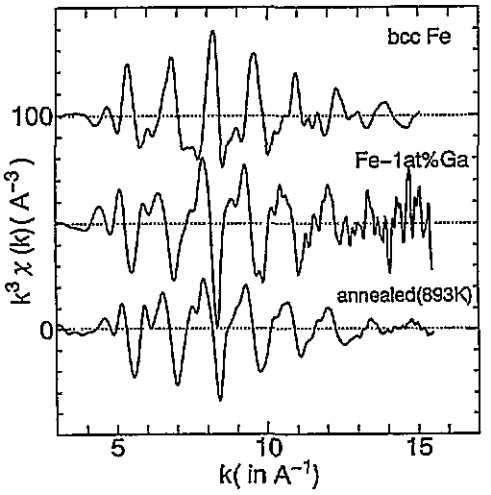

Figure 5. Comparison of $k^3\chi(k)$ against k curves of the Ga K edge among those of pure bcc Fe, $Fe_{99}Ga$ and the $Fe_{73}Ga_4Nb_3Si_{11}B_9$ annealed at 893 K.

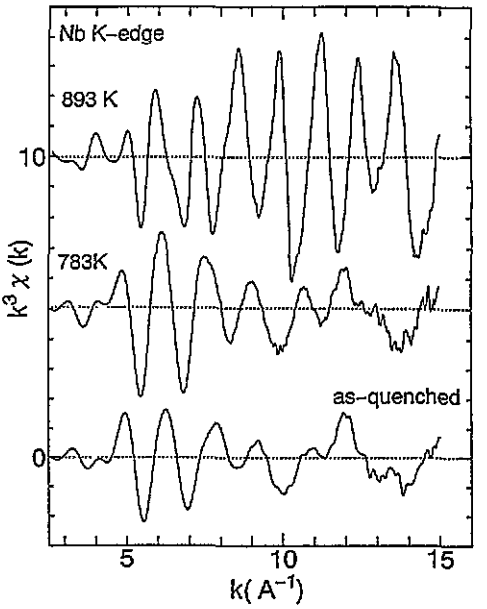

Figure 6. $k^3\chi(k)$ against k curves of the Nb K edge for the sample as quenched and annealed at 783 K and 893 K of $Fe_{73}Ga_4Nb_3Si_{11}B_9$.

annealed samples below T_{x1} as well as as-quenched one; $A_i(k)$ and $\Phi_i(k)$ in equation (1) are modified as follows for the curve fitting of the amorphous phase.

$$A_i(k) = \frac{N_i}{kr_i^2} f_i(k) \exp\left[-\frac{2r_i}{\lambda} - 2C_2k^2 + \tfrac{2}{3}C_4k^4\right] \tag{2}$$

$$\Phi_i(k) = 2kr_i - \tfrac{4}{3}C_3k^3 + \phi_i(k) \tag{3}$$

where C_2 is mean square radial displacement (Debye–Waller factor) and C_3 and C_4 the third- and fourth-order moments respectively. Curve fitting analysis was done for the observed $k^3\chi(k)$ which is inverse transformed from the Fourier-filtered radial structure function. The Fourier-filtered r range is $1.0 \leqslant r \leqslant 3.0$ Å which is displayed in figure 4 by a dotted line. The curve fitting k range is chosen from 2.6 to 15.5 $Å^{-1}$. Two shells were adopted for the curve fitting analysis of annealed samples above T_{x1} where α-iron is precipitated. The curve-fitted result is shown in figure 7 together with the observed one for FeGaNbSiB, annealed at 893 K, as an example. Structural parameters deduced by curve fitting of the $k^3\chi(k)$ for FeNbSiB, as quenched and annealed at 623 K, 693 K, 713 K, 723 K, 783 K and 893 K, are listed in table 1 together with those of $Fe_{99}Ga$ and bcc iron as references. The R factor in table 1 is defined as follows:

$$R \text{ factor} = \left(\int_{k_{min}}^{k_{max}} \left|k^3\chi^{obs}(k) - k^3\chi^{cal}(k)\right|^2 \, dk\right) \Big/ \int_{k_{min}}^{k_{max}} \left|k^3\chi^{obs}(k)\right|^2 \, dk. \tag{4}$$

The results of atomic distance r, coordination number N and mean square radial displacement C_2 are shown in figures 8, 9 and 10 as a function of annealing temperature respectively. Though the nearest-neighbour distance r_1 keeps constant after annealing, N

Table 1. Curve fitting results of $k^3\chi(k)$ for the Ga K edge of $Fe_{73}Ga_4Nb_3Si_{11}B_9$. A one-shell model was adopted for the samples as quenched and annealed below T_{x1} (=723 K), and a two-shell model for the samples annealed above T_{x1} and $Fe_{99}Ga$. r_1, r_2: distances of the first and the second shell from a central Ga atom respectively. N_1, N_2: coordinations for the first and the second shell respectively. C_{21}, C_{22}: second-order cumulants (mean square radial displacement) for the first and the second shell respectively. C_3, C_4: third- and fourth-order cumulants. R factor: reliability factor defined in the text.

	r_1 (Å)	r_2 (Å)	N_1	N_2	C_{21} (Å^2)	C_{22} (Å^2)	$C_3 \times 10^3$ (Å^3)	$C_4 \times 10^4$ (Å^4)	R factor
As-quenched	2.54 ± 0.02		8.3 ± 0.5		0.012 ± 0.001		0.67 ± 0.02	0.20 ± 0.02	1.36×10^{-2}
623 K	2.54 ± 0.02		9.2 ± 0.5		0.014 ± 0.001		0.50 ± 0.02	0.60 ± 0.02	3.33×10^{-2}
693 K	2.51 ± 0.02		8.8 ± 0.5		0.014 ± 0.001		0.30 ± 0.02	0.80 ± 0.02	1.99×10^{-2}
713 K	2.53 ± 0.02		9.4 ± 0.5		0.014 ± 0.001		0.34 ± 0.02	1.01 ± 0.02	1.99×10^{-2}
723 K	2.51 ± 0.02		6.8 ± 0.5		0.010 ± 0.001		0.13 ± 0.02	0.41 ± 0.02	2.61×10^{-2}
783 K[a]	2.50 ± 0.02	2.83 ± 0.02	7.6 ± 0.5	6.2 ± 0.5	0.0040 ± 0.0007	0.0076 ± 0.0007			1.01×10^{-2}
893 K[a]	2.50 ± 0.02	2.82 ± 0.02	7.3 ± 0.5	7.7 ± 0.5	0.0041 ± 0.0007	0.0067 ± 0.0007			1.45×10^{-2}
$Fe_{99}G$[a]	2.50 ± 0.02	2.87 ± 0.02	6.6 ± 0.5	4.5 ± 0.5	0.0018 ± 0.0007	0.0036 ± 0.0007			2.45×10^{-2}
bcc-Fe[b]	2.4838	2.8664	8	6					

[a] Two-shell model.
[b] From x-ray data.

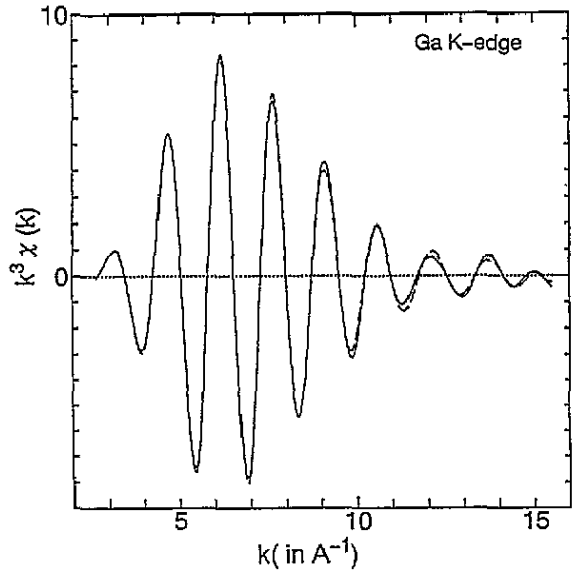

Figure 7. Comparison of the Fourier-filtered $k^3\chi(k)$ against k curves of the Ga K edge between the curve fitted results and observed ones. A solid line indicates the observed one for the as-quenched $Fe_{73}Ga_4Nb_3Si_{11}B_9$. A broken line indicates the curve-fitted one.

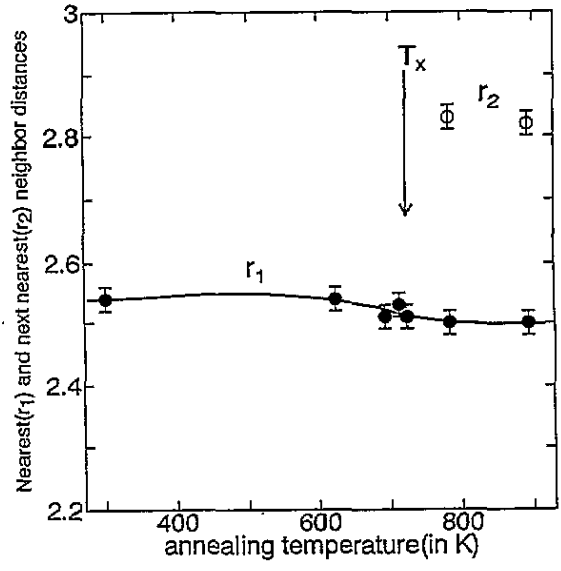

Figure 8. Nearest-neighbour distances (r_1) deduced by the curve fitting of $k^3\chi(k)$ for the Ga K edge in $Fe_{73}Ga_4Nb_3Si_{11}B_9$ as a function of annealing temperature. Next-neighbour distances (r_2) are also shown by open circles for those annealed at above T_{x1}.

and C_2 show a discontinuous change at around the precipitation temperature of α-iron (T_{x1} = 723 K). The coordination number N increases slightly with increasing annealing temperature up to 713 K and drops at T_{x1}. It rapidly increases again at above T_{x1} forming a steep dip at T_{x1}. A significant decrease at T_{x1} is observed for C_2. Above T_{x1}, C_{21} (C_2 for the first shell) decreases further. These characteristic features do not depend much on

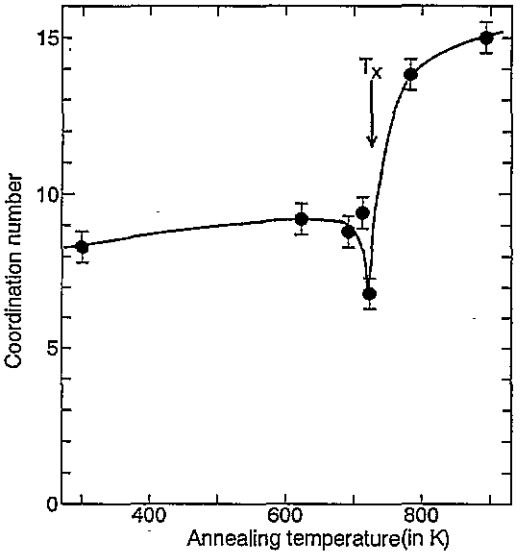

Figure 9. The coordination numbers of the nearest-neighbour atoms deduced by the curve fitting of $k^3\chi(k)$ for the Ga K edge in $Fe_{73}Ga_4Nb_3Si_{11}B_9$ as a function of annealing temperature. The values for those above T_{x1} are sum of those in first and the second shells.

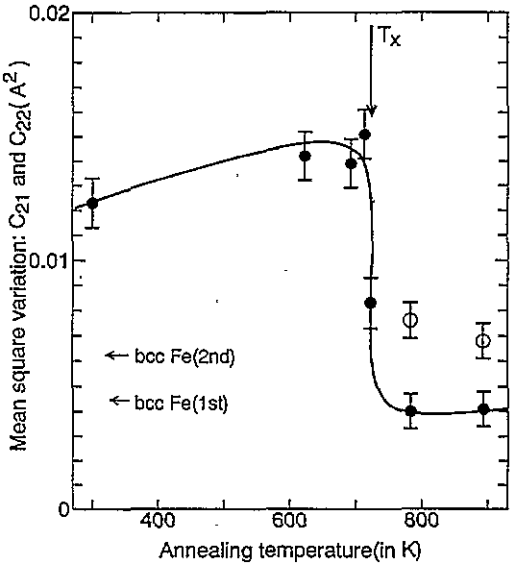

Figure 10. The mean square radial displacement for the first shell deduced by the curve fitting of $k^3\chi(k)$ for the Ga K edge in $Fe_{73}Ga_4Nb_3Si_{11}B_9$ as a function of annealing tempera- ture. Open cicles above T_{x1} are those for the second shell.

the number of shells used in the curve fitting analyses, i.e. whether one shell (fcc iron) or two shells (bcc iron) for those annealed below T_{x1}. Furthermore curve fitting results using the cumulant method do not differ much from those using a Gaussian distribution. Therefore, the anharmonicity of radial displacement in the present amorphous alloys is not so significant as those reported previously, e.g. amorphous Fe–B (Crescenzi *et al* 1981) and

or Cu–Zr (Sadoc *et al* 1984) alloys.

5. Discussion

The XAFS results of the Ga and the Nb K edges for $Fe_{73}Ga_4Nb_3Si_{11}B_9$ show that the local structure change of Ga during the crystallization is directly related to the precipitation of α-iron but not with the Fe–B compound formation. On the other hand the local structure change of Nb is strongly correlated with the Fe–B compound formation but not with the α-iron precipitation. The local structure of Ga of the sample annealed at above T_{x1} (=723 K) is quite similar to that of Ga in crystalline $Fe_{99}Ga$.

The curve fitting results for Ga in FeGaNbSiB at various annealing temperatures show that some structural rearrangements develop when the annealing temperature is close to T_{x1}. A slight drop of mean square radial displacement C_2 at T_{x1} reflects the fact that the transition from amorphous to crystalline state of the Ga local structure has started but not completed yet. It seems strange that the coordination number drops sharply at T_{x1} but it rises again up to the value close to that of α-iron by further high-temperature annealing. As we assume neighbouring atoms around Ga are iron in the curve fitting analysis, the decrease in the coordination number suggests that the number of lighter atoms (*B is more likely than Si*) around Ga increases at T_{x1}. Therefore, at an early stage of α-iron precipitation, Ga atoms can move toward the surface of a grain, i.e. grain boundaries where lighter atoms of Si and B are much abundant. An alternative explanation of the transient decrease in coordinations at T_{x1} is that at the beginning of α-iron precipitation Ga is dragged toward α-iron grains because of the negative heat of formation between Fe and Ga, i.e. -8 J mol^{-1} (de Boer *et al* 1988). Because the drop of coordination number is observed at the very limited annealing temperature at T_{x1}, such a Ga exclusion or segregation near grain boundaries occurs transiently just at the beginning of α-iron precipitation. After this transient segregation, they dissolve into α-iron with further grain growth. The enrichment with Ga at the boundaries between α-iron nuclei and surrounding amorphous matrix can reduce interface energy, which may lower the critical radius of nucleation. Consequently such a transient segregation of Ga lowers the precipitation temperature of α-iron. At the present time it cannot be concluded whether Ga atoms are excluded or dragged toward the grain surface and why this happens just at the beginning of precipitation.

The curve fitting results of Ga for the sampled annealed at 893 K are quite like those of $Fe_{99}Ga$. Some small discrepancies in the XAFS results of the Ga K edge between FeGaNbSiB (annealed at 893 K) and $Fe_{99}Ga$ can be attributed to the Si and B dissolved in the precipitated α-iron. Model calculations using FEFF5 for some Fe–Ga and Fe–B compounds in which a Ga atom sits substitutionarily at an Fe site show a large discrepancy between the calculated and the observed behaviour. These calculations lead to both of compound formation of Fe–Ga and inclusion of Ga into Fe–B being ruled out.

6. Summary

XAFS results of Ga in FeGaNbSiB show that local structure of Ga does not change significantly by annealing below T_{x1} unlike Cu in FINEMET though Ga plays the same role as Cu in the nanocrystalline formation. Curve fitting analyses of the Ga K edge XAFS show that the coordinations around Ga atoms decrease at the very beginning of α-iron precipitation although they increase up to a value close to that of bcc Fe by further annealing. Because Ga is dissolved after annealing at above T_{x1}, this decrease in coordination can be attributed

to the transient segregation of Ga toward grain boundaries just at the beginning of α-iron precipitation. This transient segregation of Ga at the interface may reduce the surface energy of α-iron nuclei and eventually lower the precipitation temperature of α-iron. XAFS results of Nb in FeGaNbSiB are very similar to that in FINEMET. Nb can be considered as playing the same role as that in FINEMET.

Acknowledgments

The present work has been carried out under approval of the Photon Factory Program Advisory Committee (acceptance No 93G045). One of the authors, M Matsuura, owes this work to the financial support by a grant-in-aid for scientific research, project No 06650735, from the Ministry of Education, Japan.

References

Bunker G 1983 *Nucl. Instrum. Methods.* **207** 437–41
Crescenzi M, Balzarotti A, Comin F, Incoccia L, Mobilio S and Motta N 1981 *Solid State Commun.* **37** 921–3
de Boer F R, Boom R, Mattens W C M, Miedema A R and Niessen A K 1988 *Cohesion in Metals—Transition Metal Alloys* (Amsterdam: North-Holland)
Eisenberger P and Brown B S 1979 *Solid State Commun.* **29** 481–4
Kataoka N, Matsunaga T, Inoue A and Masumoto T 1989 *Mater. Trans. JIM* **30** 947–50
Kim S-H, Matsuura M, Sakurai M and Suzuki K 1993 *Japan. J. Appl. Phys.* **32** 676–8
Köster U and Herold U 1981 *Glassy Metals: Springer Topics in Applied Physics* ed H-J Guntherodt and H Beck (Berlin: Springer) pp 225–59
Rehr J I, Mustre J, Zabinsky S T and Albers R C 1991 *J. Am. Chem. Soc.* B **11** 5135–40
Sadoc A, Calvayrac Y, Quivy A, Harmelin M and Flank A M 1984 *J. Non-Cryst. Solids* **65** 109–29
Tomida T 1994 *Mater. Sci. Eng.* A **179/180** 521–5
Yoshizawa Y, Oguchi S and Yamauchi K 1988 *J. Appl. Phys.* **64** 6044–6
Yoshizawa Y and Yamauchi K 1990 *Mater. Trans. JIM* **31** 307–14